J. Fluid Mech. (2005), *vol.* 526, *pp.* 361–376.
DOI: 10.1017/S0022112004003209 Printed in the United Kingdom

Turbulent entrainment in jets with arbitrary buoyancy

By EDOUARD KAMINSKI, STEPHEN TAIT AND GUILLAUME CARAZZO

Laboratoire de Dynamique des Systèmes Géologiques, Université Paris 7-Denis Diderot and Institut de Physique du Globe de Paris, 4 Place Jussieu, 75252 Paris cédex 05, France

(Received 5 December 2003 and in revised form 25 October 2004)

Explosive volcanic jets present an unusual dynamic situation of reversing buoyancy. Their initially negative buoyancy with respect to ambient fluid first opposes the motion, but can change sign to drive a convective plume if a sufficient amount of entrainment occurs. The key unknown is the entrainment behaviour for the initial flow regime in which buoyancy acts against the momentum jet. To describe and constrain this regime, we present an experimental study of entrainment into turbulent jets of negative and reversing buoyancy. Using an original technique based on the influence of the injection radius on the threshold between buoyant convection and partial collapse, we show that entrainment is significantly reduced by negative buoyancy. We develop a new theoretical parameterization of entrainment as a function of the local (negative) Richardson number that (i) predicts the observed reduction of entrainment and (ii) introduces a similarity drift in the velocity and buoyancy profiles as a function of distance from source. This similarity drift allows us to reconcile the different estimates found in the literature for entrainment in plumes.

1. Introduction

Turbulent plumes and jets are created by a maintained source of buoyancy and/or momentum at large Reynolds number. The dynamics of these flows has been a vivid source of theoretical, numerical and experimental studies in fluid mechanics since the 1950s. They represent a canonical model of free shear flow and are especially pertinent in environmental and geophysical science. Volcanic jets stand as the most energetic and dangerous turbulent flow on Earth (figure 1). They also represent a special case that can give rise to varied dynamics. Two regimes have been identified (Sparks & Wilson 1976). In the buoyant (or Plinian) regime, the initial jet is a hot dense mixture of gas and pyroclasts, but it becomes buoyant in the atmosphere owing to vigorous entrainment and heating of air, and then rises to high altitudes. In the collapse regime, the jet consumes its initial momentum before becoming buoyant and collapses to produce dangerous hot gravity currents on the local topography known as pyroclastic flows. It has been shown that the transition between these regimes is a sensitive function of the rate of entrainment of air which controls the evolution of buoyancy of the jet (Woods 1995; Kaminski & Jaupart 2001). Because of the huge fluxes involved in such flows (e.g. mass fluxes larger than $10^{10}\,\mathrm{kg\,s^{-1}}$ (Kaminski & Jaupart 2001)) the realistic prediction of their behaviour, and the safe forecasting of their consequences, require an accurate description of entrainment in physical models of volcanic jets.

At small scale, the agents of entrainment are turbulent eddies forming a mixing layer between the jet and its surroundings. Taylor (1945) and Morton, Taylor & Turner

FIGURE 1. Photograph by C. G. Newhall on 23 September 1984 of pyroclastic flows sweeping down the side of Mayon Volcano, Philippines.

(1956) were at the origin of the most successful macroscopic quantitative description of entrainment. Using a 'top-hat' formalism, in which the velocity and buoyancy force are assumed constant across the jet and zero outside it, they proposed that the entrainment rate at the edge, U_ϵ, was proportional to the average vertical velocity W,

$$U_\epsilon = \alpha_e W, \tag{1.1}$$

with α_e the entrainment constant. Numerous experimental studies provide values of entrainment constants (see Fischer *et al.* 1979; Chen & Rodi 1980; Wang & Law 2002 for reviews at different stages of the subject). The estimates vary between values as small as $\alpha_j \approx 0.07$†, for non-buoyant jets, and as large as $\alpha_p \approx 0.16$†, for buoyant plumes (Linden 2000). Although some variability can be found among the different studies, a robust result is that entrainment is always notably more efficient in buoyant plumes than in non-buoyant jets. In the case of a volcanic jet, the crucial regime is that in which the initial momentum is being consumed by the action of a negative buoyancy force. However, no values of the entrainment constant in the case of negative buoyancy can be found in the literature, and geophysicists usually use the gross approximation that $\alpha_e \approx 0.1$ (Woods & Caulfield 1992). The first aim of this paper is to provide a better estimate of the entrainment constant for negatively buoyant jets.

Various techniques can be used to estimate the entrainment constant. Early studies were based on the relationship between the opening angle of the jet and the entrainment constant. More recent studies have relied on careful measurements of the velocity and buoyancy profiles in the jets as a function of distance from the source. For jets, the different estimates converge remarkably well to an average value of $\alpha_e = 0.075 \pm 0.05$. For plumes, however, it remains difficult to cite a definitive value for the entrainment constant as the different studies give notably divergent results. The inferred value for a plume varies between 0.10 in Baines (1983) to 0.16 in Shabbir & George (1994), i.e. a 60 % variation. Such differences – usually ignored

† Values of α_e are often quoted with respect to a Gaussian profile of axial velocity, but here we convert systematically to corresponding top-hat values.

in engineering – may have non-negligible consequences in the case of the huge fluxes involved in volcanic eruptions. The variability may have different origins that are discussed in detail in Wang & Law (2002). Measurements with flying hot-wire probes apparently differ from measurements with stationary hot-wire probes that themselves differ from measurements using laser-Doppler anemometry. The fluid used and the origin (compositional or thermal) of buoyancy and the distance from the source are also put forward as possible factors giving rise to discrepancies between the results, but in unknown ways. This discussion remains largely unresolved and no convincing explanation is given for the apparent discrepancies. We propose in this paper a direct determination of the entrainment constant for negatively buoyant jets that bypasses the measurement of accurate local velocity and buoyancy profiles. Together with a self-consistent derivation of the entrainment constant as a function of buoyancy, this determination will help to reconcile the different estimates of the entrainment constant.

2. Experimental study of entrainment in negatively buoyant jets

The usual determination of the entrainment constant is based on the measurement of the velocity profiles at different heights above the source, which raises the problem of the dependence of the result on the chosen technique. Alternative approaches have been proposed to bypass the determination of accurate profiles, in which the inflow is directly measured. Such global measurements are judged as the most accurate (Turner 1973; Linden 2000). For jets, Ricou & Spalding (1961) found indeed a consistent value of $\alpha_j = 0.08$. For plumes, however, Baines (1983) found quite a small value of $\alpha_p = 0.10$. This result is smaller than the smallest value obtained from profile measurements, $\alpha_p = 0.12$ (Rouse, Yih & Humphreys 1952; Papanicolaou & List 1988), and is hardly taken into account, probably because no physical justification was given for such a finding. Here we propose also a 'bulk' determination of the entrainment, sensitive enough to contribute significantly to the debate. This method is based on the criterion for the collapse of negatively buoyant jets.

Jets with negative buoyancy will eventually collapse down to the ground once their initial momentum has been exhausted by gravity forces. Volcanic jets have the ability to reverse their buoyancy by entrainment and heating of air. If entrainment is efficient enough, the jets may then become buoyant. To study the behaviour of such jets with reversing buoyancy, Woods & Caulfield (1992) developed laboratory experiments using a mixture of methanol and ethylene glycol (MEG). This mixture is less dense than fresh water but becomes denser when mixed with more than 60 % of water. A downward propagating jet of MEG in a tank of fresh water is initially buoyant. Hence, if the entrainment of water is insufficient the jet 'collapses' to the top of the tank whereas if entrainment is efficient enough the jet becomes negatively buoyant and reaches the bottom of the tank (figure 2). Using a top-hat formalism, Woods & Caulfield (1992) expressed the criterion for collapse of the jet as an analytical relationship between the initial density anomaly of the jet, $\Delta\rho_0$, and the minimum volume flux F_m required to generate a plume,

$$\Delta\rho_0 \left[1 - \left(1 - \frac{\Delta\rho_0}{\Delta\rho_m}\right)^{1/2}\right] = \tfrac{16}{5}\alpha_e \frac{\rho_w F_m^2}{g R_0^5}, \tag{2.1}$$

where $\Delta\rho_m$ is the maximum (positive) density anomaly a mixture of MEG and water can reach, R_0 is the initial jet radius, ρ_w is the density of fresh water and g is gravity. The experiments were performed for a constant R_0, for initial dimensionless density

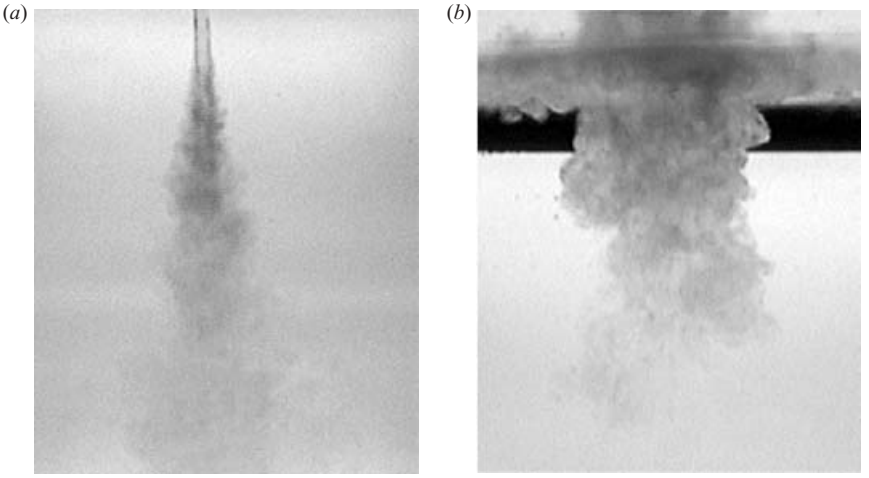

FIGURE 2. Video image of turbulent jets in (*a*) 'buoyant' and (*b*) collapse regimes.

anomalies $\Delta\rho_0/\Delta\rho_m$ varying between 1 and 6, and for volume fluxes varying between 2 and 12 $\mathrm{cm}^3\,\mathrm{s}^{-1}$. Using an average value of 0.1 for the entrainment constant, they showed a satisfactory agreement between the threshold volume flux measured in the experiments and the top-hat prediction. However, the small range of experimental conditions was not sufficient to provide an accurate determination of the entrainment constant.

We can note in (2.1) that the initial vent radius appears with the largest power, a power of 5. The solution is then much more sensitive to the initial radius than to the initial density anomaly. We thus performed a new set of experiments based on the same principle, but keeping a constant initial density anomaly and systematically varying the initial radius. To generate a forced plume with a reversing buoyancy, we used a mixture of ethanol and ethylene glycol, or EEG, which has a qualitatively similar behaviour to MEG. The precise EEG starting mixture was composed of 40 % ethanol and 60 % ethylene glycol by mass. EEG is miscible with water in all proportions and the evolution of the density of the EEG–water mixture is given in figure 3. The density is a nonlinear function of mixing ratio. Moreover, the mixture density is less than that of water when the fraction of EEG is >0.6 and greater than that of water when the fraction of EEG is <0.6. The EEG is injected from a reservoir held at a prescribed pressure through a nozzle fixed at the top of a $45 \times 45 \times 45\,\mathrm{cm}^3$ tank filled with distilled water. The mass of the EEG reservoir is monitored as a function of time to give mass and volume fluxes for each experiment (figure 4).

The jet is filmed using a video camera (figure 2). The injection device was used with different radii in order to change the momentum flux for a given overpressure and hence the conditions of collapse. For a given injection radius, the jet can be in the buoyant, total collapse or partial collapse regimes. If the volume flux is large enough, the jet becomes buoyant, whereas the jet collapses if the volume flux is too small (figure 5). When the volume flux is close to the threshold volume flux (equation (2.1)) partial collapse occurs, in which only part of the jet goes down to the bottom of the tank. As soon as partial collapse occurs, the top-hat formalism does not apply, because the jet is not in steady state. We put partial collapse in the collapsing regime in order to compare experiments with theory. For each experiment, the jet was not fully turbulent at the nozzle – its exterior remained smooth and cylindrical for distances of

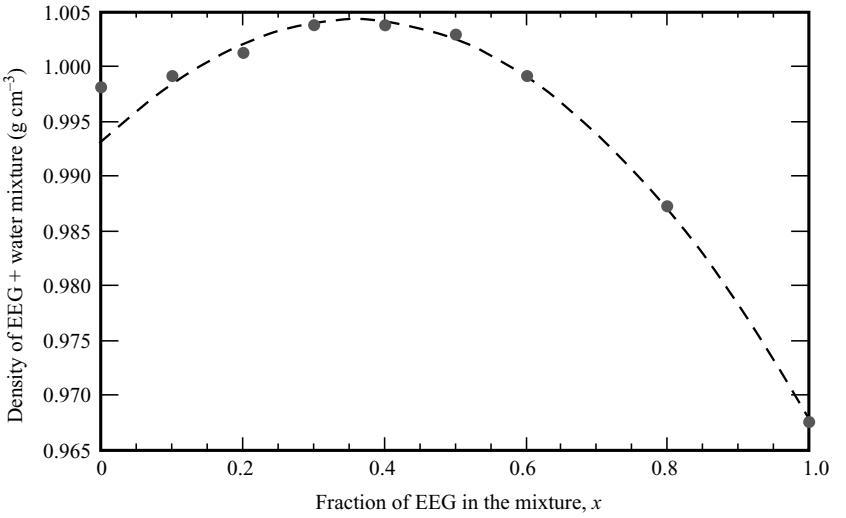

FIGURE 3. Evolution of the density of the mixture between EEG and water. The circles are measurements, whereas the dashed line is the polynomial fit used for numerical calculation. For concentrations of water larger than 0.6, the mixture becomes denser than water.

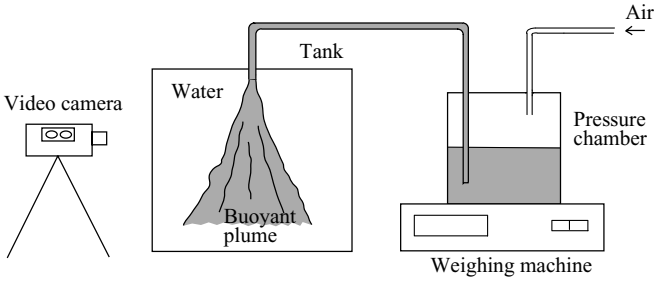

FIGURE 4. Experimental apparatus.

the order of a centimetre. We measured from video images the effective radius R_f of the jet at which it becomes rough and irregular, i.e. at which turbulent entrainment began. The parameters for each experiment are given in table 1.

The raw output of the experiments is then a regime diagram of the jet (collapsing fountain or buoyant plume) as a function of the effective radius and of the initial volume flux. According to (2.1), in a graph $F_o = f(R_0^{2.5})$ the threshold between the two regimes is a straight line, the slope of which is proportional to the square root of the entrainment constant α_e. We plot our experimental results in such a diagram (figure 6) and compare the threshold condition with that obtained with the reference value of the entrainment constant used for negatively buoyant volcanic jets ($\alpha_e = 0.1$). This value of α_e clearly underestimates the threshold fluxes for collapse, which shows that the entrainment is reduced in a negatively buoyant plume. The best agreement between the experiments and the theoretical prediction is obtained for $\alpha_e = 0.057$.

In each experiment, we determined the regime, which can be done without ambiguity, and measured two variables: mass flux at the input nozzle and effective initial radius. The former is measured using an accurate weighing balance, while the latter is measured precisely from video images using standard high-resolution image

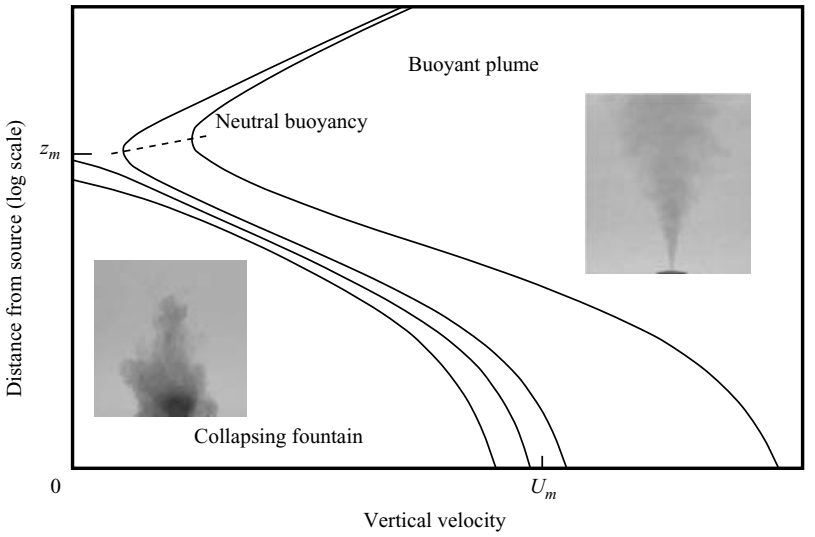

FIGURE 5. Qualitative diagram illustrating the principles of determination of the maximal (threshold) volume flux for collapse. For a given initial radius R_0, collapse occurs for volume flux smaller than the threshold flux F_m (or here for an initial velocity smaller than $U_m \equiv F_m/R_0^2$).

Experiment number	F_0 (cm^3 s^{-1})	R_0 (cm)	R_f (cm)	Re	Ri	Regime
6	2.50	0.300	0.74	833	−0.107	collapse
7	3.14	0.300	0.44	1047	−0.005	plume
8	1.71	0.300	0.59	570	−0.073	collapse
9	1.71	0.300	0.46	570	−0.021	collapse (p)
16	20.41	0.605	0.74	3402	−0.002	plume
17	9.55	0.605	0.77	1592	−0.009	collapse (p)
18	18.83	0.605	0.86	3138	−0.004	plume
19	13.74	0.605	0.87	2290	−0.008	plume
20	10.43	0.605	0.99	1738	−0.026	collapse (p)
21	22.79	0.605	0.81	3798	−0.002	plume
22	19.76	0.605	0.86	3293	−0.004	plume
23	6.72	0.605	0.77	1120	−0.018	collapse
24	6.82	0.605	0.82	1137	−0.024	collapse (p)
25	9.19	0.605	0.76	1532	−0.009	collapse (p)
33	8.07	0.605	0.87	1345	−0.023	collapse (p)
34	5.32	0.605	0.95	887	−0.082	collapse
35	4.51	0.300	0.43	1503	−0.002	plume
36	3.39	0.300	0.54	1130	−0.012	plume
37	2.57	0.300	0.49	857	−0.013	plume
38	1.49	0.300	0.51	497	−0.047	collapse
39	1.80	0.300	0.53	600	−0.039	collapse (p)
40	0.89	0.200	0.46	445	−0.078	plume
41	0.73	0.200	0.43	365	−0.083	collapse
42	0.86	0.200	0.43	430	−0.060	collapse
45	3.78	0.405	0.64	945	−0.023	collapse
46	4.77	0.405	0.72	1193	−0.026	collapse (p)
47	5.68	0.405	0.66	1420	−0.012	plume

TABLE 1. Experimental conditions. Cases of partial collapse are referred to as collapse (p).

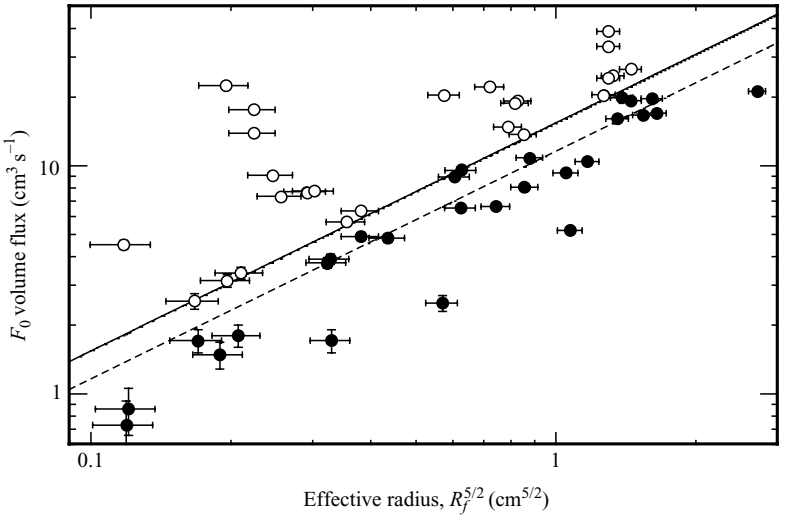

FIGURE 6. Comparison of conditions for collapse in laboratory experiments and according to the analytical prediction of (2.1.) Solid circles correspond to jets in the collapse regime, and open circles correspond to jets in the buoyant regime. The dashed line gives the theoretical prediction for the value of the entrainment constant typically used for volcanic negatively buoyant plumes ($\alpha_e = 0.1$), whereas the solid line shows the best fit obtained for $\alpha_e = 0.057$.

analysis software. Both measurements are accurate, and the method gives a robust result because we avoid the technically very difficult procedures involved in measuring precise profiles of flow variables. The error bars on the regime diagram clearly show that the reduced value of α_e is meaningful and must be accounted for.

The value of the entrainment constant, $\alpha_e = 0.057$, is the smallest ever found in the literature on classical non-buoyant jets and positively buoyant plumes. This value is, indeed, not only much smaller than the values inferred for positively buoyant plumes (by a factor of 2–3), but also significantly smaller than the value found for non-buoyant jets ($\alpha_j = 0.075$). Values as small as ours have been proposed only for the very specific case of volumetrically heated jets (Bhat & Narasimha 1996). For these flows, the increase of buoyancy by volumetric heating is supposed to be responsible for the entrainment deficiency. In our case, however, buoyancy is negative and the link between the two observations is not straightforward. The question reduces then to the role played by buoyancy in the reduction of entrainment, and a detailed physical parameterization of entrainment is necessary to understand their relationship.

3. A theoretical model of entrainment for negatively buoyant plumes

3.1. *Parameterization of entrainment as a function arbitrary buoyancy*

The larger entrainment in plumes than in jets is usually interpreted as an effect of buoyancy-induced turbulence. Two parameterizations have been proposed to account for this effect. The first one is purely empirical (Fischer *et al.* 1979)

$$\alpha_e = \alpha_j \exp\left[\ln\left(\frac{\alpha_p}{\alpha_j}\right)\left(\frac{Fr_p}{Fr}\right)^2\right], \tag{3.1}$$

Symbol	Variable
r	Distance from the axis
z	Distance from the source
$u = \overline{u} + \tilde{u}$	Radial velocity
$w = \overline{w} + \tilde{w}$	Vertical velocity
$g' = \overline{g'} + \tilde{g'}$	Reduced gravity
$\overline{u}$	Reynolds-averaged radial velocity
$\overline{w}$	Reynolds-averaged vertical velocity
$\overline{g'}$	Reynolds-averaged reduced gravity
$\tilde{u}$	Turbulent fluctuations of radial velocity
$\tilde{w}$	Turbulent fluctuations of vertical velocity
$\tilde{g'}$	Turbulent fluctuations of reduced gravity
$-\rho\overline{\tilde{u}\tilde{w}}$	Turbulent shear stress
Q	Mass flux
M	Momentum flux
B	Buoyancy flux
R	Top-hat radial length scale
W	Top-hat vertical velocity scale
G'	Top-hat reduced gravity scale
b_m	Lateral extent of the jet
w_m	Axial vertical velocity
g'_m	Axial reduced gravity
$f(r, z)$	Velocity shape function
$h(r, z)$	Buoyancy shape function
$j(r, z)$	Turbulent shear stress shape function
Ri	Richardson number
Re	Reynolds number

TABLE 2. Notation.

with Fr_p the Froude number of a plume. The second one is semi-empirical and inspired by the theoretical work of Priestley & Ball (1955)

$$\alpha_e = \alpha_j + (\alpha_p - \alpha_j)\left(\frac{Fr_p}{Fr}\right)^2. \tag{3.2}$$

Although these equations predict successfully the change of entrainment between jets and plumes (Wang & Law 2002), their physical basis is not clear and they can be seen as more useful than meaningful. To gain some insight into the physics hidden behind these parameterizations, we propose to revisit the work of Priestley & Ball (1955).

We first write down mass, momentum and buoyancy conservation for a ring-shaped volume of an axisymmetric turbulent buoyant jet, in Boussinesq approximation and steady state,

$$\frac{\partial}{\partial z}(r\overline{w}) + \frac{\partial}{\partial r}(r\overline{u}) = 0, \tag{3.3}$$

$$\frac{\partial}{\partial z}(r\overline{w}^2) + \frac{\partial}{\partial r}(r\overline{u}\,\overline{w}) = r\overline{g'} - \frac{\partial}{\partial r}(r\overline{\tilde{u}\tilde{w}}), \tag{3.4}$$

$$\frac{\partial}{\partial z}(r\overline{w}\,\overline{g'}) + \frac{\partial}{\partial r}(r\overline{u}\,\overline{g'}) = 0, \tag{3.5}$$

using the notation given in table 2. All quantities relate to mean values for the ring obtained by Reynolds-averaging (Hinze 1975). As in Morton (1971) we neglect all contributions from turbulent fluctuations in velocity and reduced gravity which are

of second order. The turbulent shear stress $-\rho\overline{\tilde{u}\tilde{w}}$ (which drives entrainment) is of leading order. From mass and momentum conservation, we then derive the balance equation for the kinetic-energy of axial mean motion,

$$\frac{\partial}{\partial z}\left(\tfrac{1}{2}r\overline{w}^3\right)+\frac{\partial}{\partial r}\left(\tfrac{1}{2}r\overline{u}\,\overline{w}^2\right)=r\overline{w}\overline{g'}-\overline{w}\frac{\partial}{\partial r}(r\overline{\tilde{u}\tilde{w}}). \tag{3.6}$$

Integrating these equations from $r=0$ to ∞ taking as boundary conditions $\lim_{r\to\infty} r\overline{u}\,\overline{w}=\lim_{r\to\infty} r\overline{\tilde{u}\tilde{w}}=\lim_{r\to\infty} r\overline{u}\overline{g'}=0$, yields

$$\frac{\mathrm{d}}{\mathrm{d}z}\int_0^\infty r\overline{w}^2\,\mathrm{d}r=\int_0^\infty r\overline{g'}\,\mathrm{d}r, \tag{3.7}$$

$$\frac{\mathrm{d}}{\mathrm{d}z}\int_0^\infty r\overline{w}\overline{g'}\,\mathrm{d}r=0, \tag{3.8}$$

$$\frac{\mathrm{d}}{\mathrm{d}z}\int_0^\infty \tfrac{1}{2}r\overline{w}^3\,\mathrm{d}r=\int_0^\infty r\overline{w}\overline{g'}\,\mathrm{d}r+\int_0^\infty r\overline{\tilde{u}\tilde{w}}\frac{\partial\overline{w}}{\partial r}\,\mathrm{d}r. \tag{3.9}$$

We then define a top-hat using the momentum and buoyancy fluxes, and the reduced gravity,

$$R^2W^2=\int_0^\infty r\overline{w}^2\,\mathrm{d}r, \tag{3.10}$$

$$R^2G'=\int_0^\infty r\overline{g'}\,\mathrm{d}r, \tag{3.11}$$

$$R^2WG'=\int_0^\infty r\overline{w}\overline{g'}\,\mathrm{d}r. \tag{3.12}$$

Note that we do not use the mean kinetic energy flux to define one of the top-hat integrals but rather the total buoyancy force. This allows us to recover a momentum equation identical to the one used in Morton *et al.*'s (1956) formalism, whereas in Priestley & Ball (1955) an additional constant is introduced in the momentum flux conservation. We now look for an expression for the energy flux by introducing three shape functions,

$$\overline{w}(r,z)=w_m(z)f(r,z), \tag{3.13}$$

$$\overline{g'}(r,z)=g'_m(z)h(r,z), \tag{3.14}$$

$$\overline{\tilde{u}\tilde{w}}(r,z)=-\tfrac{1}{2}w_m(z)^2j(r,z). \tag{3.15}$$

Note that at this point we do not make any assumption about self-similarity of the flow. The shape functions are then used to define five integral profiles that arise in (3.7)–(3.9),

$$I_1=\int_0^\infty r^*f(r^*,z)h(r^*,z)\,\mathrm{d}r^*, \tag{3.16}$$

$$I_2=\int_0^\infty r^*h(r^*,z)\,\mathrm{d}r^*, \tag{3.17}$$

$$I_3=\int_0^\infty r^*f(r^*,z)^2\,\mathrm{d}r^*, \tag{3.18}$$

$$I_4=\int_0^\infty r^*f(r^*,z)^3\,\mathrm{d}r^*, \tag{3.19}$$

$$I_5 = \int_0^\infty r^* j(r^*, z) \frac{\partial f}{\partial r^*} \, \mathrm{d}r^*, \tag{3.20}$$

where $r^* = r/b_m$, with b_m a radius scale. These integral profiles provide the relation between the 'notional' top-hat value and the 'real' value of the different variables,

$$R = \frac{I_3^{0.5} I_2}{I_1} b_m, \tag{3.21}$$

$$W = \frac{I_1}{I_2} w_m, \tag{3.22}$$

$$G' = \frac{I_1^2}{I_2 I_3} g'_m. \tag{3.23}$$

Using the integral profiles, we can rewrite the conservation of kinetic energy (equation (3.9)) as

$$\frac{\mathrm{d}}{\mathrm{d}z} R^2 W^3 = \frac{2}{A} R^2 W G' - R^2 W^3 \frac{\mathrm{d} \ln A}{\mathrm{d}z} - C W^3 R, \tag{3.24}$$

where A and C are combinations of the various integral profiles,

$$A = \frac{I_2 I_4}{I_1 I_3}, \tag{3.25}$$

$$C = \frac{I_2 I_3^{0.5} I_5}{I_1 I_4}. \tag{3.26}$$

We then express the mass conservation as a function of the energy flux as in Priestley & Ball (1955),

$$\frac{\mathrm{d}}{\mathrm{d}z} R^2 W = -\frac{1}{W^2} \frac{\mathrm{d}}{\mathrm{d}z} R^2 W^3 + \frac{2 R^2 G'}{W}, \tag{3.27}$$

in which we used the top-hat version of the momentum flux conservation (equation (3.7)),

$$\frac{\mathrm{d}}{\mathrm{d}z} R^2 W^2 = R^2 G'. \tag{3.28}$$

Substituting the energy flux by its expression as a function of A and C we finally obtain Morton *et al.* (1956)-like top-hat conservation equations, explicitly including mass flux conservation,

$$\frac{\mathrm{d}}{\mathrm{d}z} R^2 W = 2 R W \left[Ri \left(1 - \frac{1}{A} \right) + \tfrac{1}{2} R \frac{\mathrm{d} \ln A}{\mathrm{d}z} + \tfrac{1}{2} C \right], \tag{3.29}$$

$$\frac{\mathrm{d}}{\mathrm{d}z} R^2 W^2 = R^2 G', \tag{3.30}$$

$$\frac{\mathrm{d}}{\mathrm{d}z} R^2 W G' = 0, \tag{3.31}$$

where Ri is the local Richardson number defined as

$$Ri \equiv \frac{R G'}{W^2}. \tag{3.32}$$

The resulting equation of mass flux conservation, (3.29), gives an explicit expression for the entrainment constant,

$$\alpha_e \equiv Ri\left(1-\frac{1}{A}\right)+\tfrac{1}{2}R\frac{\mathrm{d}\ln A}{\mathrm{d}z}+\tfrac{1}{2}C, \tag{3.33}$$

as a function of integral parameters A and C.

The parameterization we have obtained is close to the more classical linear dependence of entrainment on Ri (equation (3.2)). Our formula, however, provides a physical interpretation of the different terms involved in the formula. In order to interpret the expression of the entrainment constant given in (3.33), it is useful to write A and C in alternative forms,

$$A=\frac{\displaystyle\int_0^\infty \tfrac{1}{2}r\bar{w}^3\,\mathrm{d}r}{\tfrac{1}{2}R^2W^3}, \tag{3.34}$$

$$C=\frac{R}{b_m}\frac{\displaystyle\int_0^\infty r^* j\frac{\partial f}{\partial r^*}\,\mathrm{d}r^*}{\displaystyle\int_0^\infty r^* f^3\,\mathrm{d}r^*}. \tag{3.35}$$

C is revealed as the ratio between the energy dissipated by turbulent stress, i.e. transferred from the kinetic energy of mean motion to the fluctuating velocity field via the action of turbulent stress, over the total flux of mean kinetic energy. In other words, C gives the fraction of the total energy flux available for entrainment. The parameter A reflects the influence of the shape of the velocity profile on the transfer of gravitational energy to turbulent stress via the local Richardson number. For purely top-hat profiles, $A=1$ and we retrieve the mass flux conservation used by Morton *et al.* (1956). In that case, however, (3.33) predicts $\alpha_j=\alpha_p=C/2$. This is not consistent with the observation that entrainment is larger in plumes than in jets. For Gaussian profiles, A can be expressed as a function of λ, the ratio of the half-width of the buoyancy profile over the half-width of the velocity profile,

$$A=\tfrac{2}{3}(\lambda^2+1). \tag{3.36}$$

If λ is constant and larger than $1/\sqrt{2}$, A is also constant, and larger than 1. Our parameterization is then equivalent to linear equation (3.2) and provides an explanation for the greater entrainment in plumes because they have a positive Richardson number. If the flow is not completely self-similar, however, the value of A does not have to be constant. In that case, an intriguing third term also appears in the parameterization of entrainment, $R/2\,(\mathrm{d}\ln A/\mathrm{d}z)$, which encompasses the similarity hypothesis. This term has not been recognized in the literature before and will require a more detailed discussion on its own.

3.2. *Experimental determination of the parameterization of entrainment*

The actual values of the parameters A and C (and maybe their variation) are the key parameters of the entrainment process. They cannot be obtained directly by theory, but can be estimated from laboratory experiments on positively buoyant plumes. We have reviewed the literature on the subject, with special care given to the studies in which the profiles of velocity, buoyancy and turbulent stresses are provided. All the profiles we have used are given far from the source as measured in terms of the classical 'jet

Reference	A	C	λ	z/R_0
Schmidt (1941)	1.23	—	0.92	14.5
Rouse, Yih & Humphreys (1952)	1.60	—	1.24	75
Nakagome & Hirita (1977)	1.18	—	0.88	11.5
George, Alpert & Tamanini (1977)	1.10	—	0.92	8–16
Papanicolaou & List (1988)	1.46	0.11	1.07	22–80
Panchapakesan & Lumley (1993)	1.90	0.10	1.24	90–120
Shabbir & George (1994)	1.10	0.14	0.92	10–28
Wang & Law (2002)	1.45	0.14	1.04	31–55

TABLE 3. Values of A and C inferred from literature. Values for Schmidt (1941), Rouse *et al.* (1952) and Nakagome & Hirita (1977) are calculated from Gaussian fits of the velocity and buoyancy profiles, whereas other values are obtained from best fits of the profiles. The ratio of the buoyancy to velocity half-widths is obtained assuming Gaussian profiles.

length' l_m (Fischer *et al.* 1979)

$$l_m = \frac{M_o^{5/4}}{B_o^{1/2}}, \tag{3.37}$$

and can be defined as 'pure plumes'. In Panchapakesan & Lumley (1993), the regime is more intermediate as $z/l_m \approx 2$. This study corresponds, however, to the largest value of z/D and is kept for the sake of the argument. We fitted the profiles by the following forms using the method of least-squares residual:

$$f(\eta) = \exp(a_1\eta + a_2\eta^2 + a_3\eta^3), \tag{3.38}$$

$$h(\eta) = \exp(b_1\eta + b_2\eta^2 + b_3\eta^3), \tag{3.39}$$

$$j(\eta) = -2c_o[\exp(-c_1(\eta - c_2)) - \exp(-c_1(\eta - c_2))], \tag{3.40}$$

where $\eta = r/z$ and a_i, b_i, c_i are fitting parameters. The corresponding values obtained for A and C are given in table 3.

We can see from the table that the value of C is constant (0.12 ± 0.02). Using this value for C in (3.33), we obtain $\alpha_j = 0.06 \pm 0.01$ for a pure momentum jet (i.e. for $Ri = 0$). This value is very close to the reference value of 0.07 ± 0.01. This observation is in line with the previous finding that the turbulent stress profile is very similar in the different studies on plumes and on jets (Papanicolaou & List 1988; Wang & Law 2002). The value of A shows, however, large variations from one study to the other, and differs by almost a factor of two between the two extreme values (1.1 deduced from Shabbir & George 1994 and 1.9 deduced from Panchapakesan & Lumley 1993). At first order, the variation of A is well correlated to the variation of λ, the ratio of the two half-widths, that can be either larger or smaller than 1. The actual value of λ relative to 1 has, in fact, always been at the heart of the debate between the different groups working on the subject and the definitive argument in favour of one particular value of λ is still lacking.

To try to provide an additional constraint on the effective value of A, we compare our experimental measurements to theoretical predictions given by (3.33) using the various values of A (and C) given in table 3. Instead of using the analytical relationship between the entrainment constant and the threshold volume flux for collapse, we took into account the dependence of α_e on Ri using a numerical scheme. At that stage, we made the hypothesis of complete similarity and kept A constant. In the numerical calculation, the conservation of weight deficiency is replaced by the conservation of

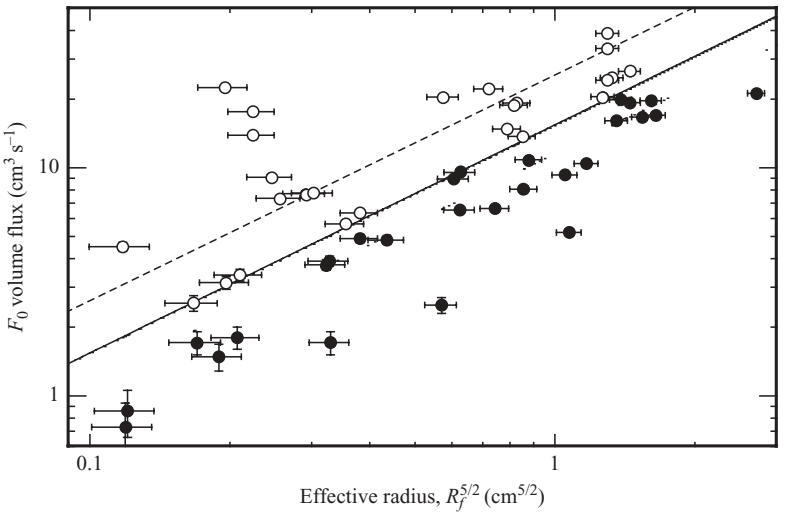

FIGURE 7. Comparison of conditions for collapse in laboratory experiments and according to turbulent jet theory. Solid circles correspond to jets in the collapse regime, and open circles correspond to jets in the buoyant regime. The dashed line gives the theoretical prediction for $A = 1.90$ and $C = 0.10$ whereas the solid line is obtained for $A = 1.10$ and $C = 0.14$.

the flux of EEG to obtain the amount x of EEG in the mixture,

$$x = x_0 \frac{W_0 R_0^2}{W R^2}, \tag{3.41}$$

where x_0 is the initial fraction of EEG and $W_0 R_0^2$ the initial volume flux. Once x is known, the density of the jet is obtained from a polynomial fit of figure 3. We solved the equations using a fourth-order Runge–Kutta scheme, looking for the threshold mass (or volume) flux at which collapse occurs. Figure 7 shows the results of the numerical calculation. We show in the figure the predictions for the two extremal parameterizations, the one deduced from Shabbir & George (1994) ($A = 1.10$, $C = 0.14$) and the one deduced from Panchapakesan & Lumley (1993) ($A = 1.90$, $C = 0.10$). It is clear from the experimental results that the values calculated for the profiles given in Shabbir & George (1994) predict the actual entrainment better. We then conclude (i) that a linear parameterization based on local Richardson number successfully reproduces the reduction of entrainment due to negative buoyancy and (ii) that λ is required to be smaller than 1 in our case. The remaining question is why our experiments are closest to the results of Shabbir & George (1994).

4. Discussion: entrainment and self-similarity drift

Because our study does not rely on actual measurements of profiles, the technique by itself is not an issue in the comparison of our results with those described in the literature. The fluid used is different in our case (water + EEG) and in Shabbir & George (1994) (heated air) and cannot be advocated in the discussion. The common point that we can identify is, however, the distance from the source. In our experiments, collapse occurs always quite close to the source ($z/R_0 \approx 20$) and the profiles were measured at similar distance in Shabbir & George (1994). In Panchapakesan & Lumley (1993) on the other hand, the measurements were made at a much larger distance ($z/R_0 \approx 100$). From that observation, we went back to the values given in

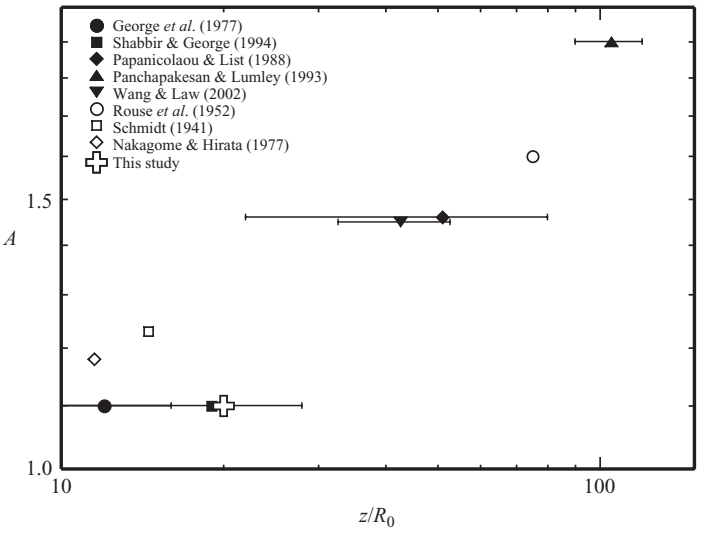

FIGURE 8. Evolution of A as a function of dimensionless distance from the source. The bars show the range of distances for each study.

table 3 and plotted the value of A as a function of the dimensionless distance from the source. The resulting plot (figure 8) shows a clear and systematic increase of A as a function of downstream distance from the source. The direct consequence of that finding is that self-similarity is not completely respected in the flows. All the authors have, however, found that the shape of both the velocity profiles and of the buoyancy profiles were themselves self-similar and close to Gaussian. The changes in A are thus only due to the change of the relative width of the two profiles that is smaller than 1 close to the source and larger than 1 far from the source. In our study, the nonlinear variation of density as a function of mixing with water may impede the development of a fully self-similar profile. However, the comparison with other experiments dealing with linear density change positively shows that the variation of A is a robust result. We propose to refer to this fact as a similarity-drift.

The second unexpected consequence of the variation of A, is that the nonlinear term that arises in our parameterization, $R/2\,\mathrm{d}\ln A/\mathrm{d}z$ is not actually zero. A rough linear regression through the points of figure 8 furthermore yields

$$\tfrac{1}{2}R\frac{\mathrm{d}\ln A}{\mathrm{d}z} \approx 10^{-3}. \tag{4.1}$$

This small similarity-drift is not large enough to be detected in a given set of experiments in which all the profiles are measured within a restricted range of z/R_0. This explains why this effect has not yet been advocated to resolve the discrepancy between the observations of the different groups. This drift is, however, large enough to explain the variability of A between the different studies.

The other case of reduced entrainment has been observed for volumetrically heated jets (Bhat & Narasimha 1996) in which entrainment can diminish to zero, even though the Richardson number is increasing. From our parameterization, it is clear that only the nonlinear term can explain such a reduction of entrainment as Ri is positive for these jets. In their study, Bhat & Narasimha (1996) found that the profiles keep a self-similar Gaussian shape before, during and after heating. They also found that λ changed from 1.25 to 1.05 during heating. From their figure 13, we calculated the

value of the nonlinear term and found

$$\tfrac{1}{2}R\frac{\mathrm{d}\ln A}{\mathrm{d}z} \approx -0.11. \tag{4.2}$$

This is larger than the value of the entrainment constant inferred by the authors before heating ($\alpha_e = 0.09$) and can explain the slightly negative entrainment constant they observed after heating. In other words, because the change of A is so abrupt in their case, the term due to the similarity-drift may even control entrainment.

The origin of the variation of λ – which induces the change in A – is beyond the scope of this paper, but we may, however, propose a sensible hypothesis. Close to the source, the buoyancy profile is narrower than the velocity profile, whereas far from the source, it is much wider. The origin of such variation might be linked to a change of the turbulent Prandtl number (or equivalently the Schmidt number) that controls the profiles in a similar way as it does for laminar plumes (Yih 1977; Kaminski & Jaupart 2003). If the turbulent Prandtl number is exactly 1, Taylor's mixing length theory predicts that the buoyancy profile follows exactly the vorticity profile. The corresponding velocity profile will be in turn $1/\sqrt{2}$ narrower than the buoyancy profile (Hinze 1975, p. 366), i.e. for Gaussian profiles $\lambda = \sqrt{2}$ and $A = 2$. Far from the source, when turbulence is fully developed, the turbulent Prandtl number should be close to 1 and it is reassuring to find that the data of Panchapakesan & Lumley (1993) give $A = 1.9$, as they are the furthest from the source. Much closer to the source, the actual value of the turbulent Prandtl number may be affected by the molecular Prandtl number which is larger than 1 and would yield velocity profiles wider than the buoyancy profiles.

5. Conclusions

We have presented the first experimental study of entrainment in jets with negative and reversing buoyancy. Using an original 'bulk' technique of determination, we have found that entrainment is much reduced by negative buoyancy.

To first order, the effect of negative buoyancy on entrainment is well described by a linear dependence of the entrainment constant on the local (negative) Richardson number. At second order, a similarity drift, corresponding to a weak evolution of the shapes and, above all, relative widths of the profiles as a function of distance from the source, must be taken into account to reconcile the various experimental studies on the subject. This nonlinear term can even explain the drastic reduction of entrainment observed in volumetrically heated jets that have been studied with application to latent heat released in convecting clouds.

The variation of entrainment with negative buoyancy may have large consequences for the dynamics of explosive eruptions. First, the conditions for collapse should be affected by the drastic reduction of entrainment close to the vent. Secondly, the entrainment in the high atmosphere and thus the maximal height reached by the eruptive column should be affected by the similarity drift identified in the present study. These consequences will be the object of a companion paper.

This paper has been much improved thanks to the editor P. Huerre and to three anonymous reviewers. The experimental device used during this study was built by Yves Gamblin at the IPGP workshop. We thank him for his enthusiasm and efficiency. The authors thank Dr C. G. Newhall for permission to use the picture of figure 1 and Pr. Law for giving us access to his data.

REFERENCES

Baines, W. D. 1983 A technique for the direct measurement of the volume flux of a plume. *J. Fluid Mech.* **132**, 247–256.

Bhat, G. S. & Narasimha, R. 1996 A volumetrically heated jet: large-eddy structure and entrainment characteristics. *J. Fluid Mech.* **325**, 303–330.

Chen, J. C. & Rodi W. 1980 *Turbulent Buoyant Jets – A Review of Experimental Data.* Pergamon.

Fischer, H. B., List, E. J., Koh, R. C. Y., Imberger, J. & Brooks, N. H. 1979 *Mixing in Inland and Coastal Waters.* Academic.

George, W. K., Alpert, R. L. & Tamanini, F. 1977 Turbulence measurements in an axisymmetric buoyant plume. *Intl J. Heat Mass Transfer* **20**, 1145–1154.

Hinze, J. O. 1975 *Turbulence.* McGraw-Hill.

Kaminski, E. & Jaupart, C. 2001 Marginal stability of atmospheric eruption columns and pyroclastic flow generation. *J. Geophys. Res.* **106**, 21 785–21 798.

Kaminski, E. & Jaupart, C. 2003 Laminar starting plumes in high-Prandtl-number fluids. *J. Fluid Mech.* **478**, 287–298.

Linden, P. F. 2000 Convection in the environment. In *Perspectives in Fluid Dynamics* (ed. G. K. Batchelor, H. K. Moffatt & M. G. Worster). Cambridge University Press.

Morton, B. R., Taylor, G. I. & Turner, J. S. 1956 Turbulent gravitational convection from maintained and instantaneous sources. *Proc. R. Soc. Lond.* A **234**, 1–23.

Morton, B. R. 1971 The choice of conservation equations for plume models. *J. Geophys. Res.* **30**, 7409–7416.

Nakagome, H. & Hirita, M. 1977 The structure of turbulent diffusion in an axizymmetric turbulent plume. *Proc. 1976 ICHMT Seminar on Turbulent Buoyant Convection*, pp. 361–372.

Panchapakesan, N. R. & Lumley, J. L. 1993 Turbulent measurements in axisymmetric jets of air and helium. Part 2. Helium Jet. *J. Fluid Mech.* **246**, 225–247.

Papanicolaou, P. N. & List, E. J. 1988 Investigations or round vertical turbulent buoyant jets. *J. Fluid Mech.* **195**, 341–391.

Priestley, C. H. B. & Ball, F. K. 1955 Continuous convection from isolated source of heat. *Q. J. R. Mech. Soc.* **81**, 144–157.

Ricou, F. P. & Spalding, D. B. 1961 Measurements of entrainment by axisymmetrical turbulent jets. *J. Fluid Mech.* **11**, 21–32.

Rouse, H., Yih, C. S. & Humphreys, H. W. 1952 Gravitational convection form a boundary source. *Tellus* **4**, 201–210.

Schmidt, W. 1941 Turbulente Ausbreitung eines Stromes erhitzter Luft. *Z. Angew. Math. Mech.* **21**, 265–278, 351–363.

Shabbir, A. & George, W. K. 1994 Experiments on a round turbulent buoyant plume. *J. Fluid Mech.* **275**, 1–32.

Sparks, R. S. J. & Wilson, C. J. N. 1976 Model for the formation of ignimbrite by gravitational column collapse. *J. Geol. Soc.* **132**, 441–456.

Taylor, G. I. 1945 Dynamics of a mass of hot gas rising in air. US Atomic Energy Commission MDDC 919. LADC 276.

Turner, J. S. 1973 *Buoyancy Effects in Fluids.* Cambridge University Press.

Wang, H. & Law, A. W.-K. 2002 Second-order integral model for a round turbulent buoyant jet. *J. Fluid Mech.* **459**, 397–428.

Woods, A. W. 1995 The fluid dynamics of explosive volcanic eruptions. *Rev. Geophys.* **33**, 495–530.

Woods, A. W. & Caulfield, C. P. 1992 A laboratory study of explosive volcanic eruptions. *J. Geophys. Res.* **97**, 6699–6712.

Yih, C.-S. 1977 Turbulent buoyant plumes *Phy. Fluids* **8**, 1234–1237.